

Supporting Information for “Long-term acceleration of aseismic slip preceding the M_w 9 Tohoku-oki earthquake: constraints from repeating earthquakes”

Contents of this file

1. Text S1 to S4
2. Table S1
3. Figures S1 to S12

Introduction

The supporting information includes four texts, one table, and eleven figures:

1. Text S1 provides details of the repeating-earthquake data selection criteria.
2. Text S2 provides details of the Mann-Kendall test.
3. Text S3 describes the different models of repeating-earthquake recurrence and provides details of the Markov-chain Monte Carlo procedure and the results of model section.

Corresponding author: A. P. Mavrommatis, Department of Geophysics, Stanford University, 397 Panama Mall, Stanford, California 94305, USA. (andream@stanford.edu)

4. Text S4 provides details of the joint GPS/repeating-earthquake inversion for slip acceleration, including details about estimating correlations in GPS station accelerations and model regularization.

5. Table S1 summarizes the result of the Mann-Kendall test.

6. Figure S1 shows the epicentral distribution of families of repeating earthquakes used in this study, highlighting those that passed our selection criteria.

7. Figure S2 summarizes statistics of the families of repeating earthquakes in terms of number of events per family and average recurrence interval, and shows that the majority of families have less than 4 events.

8. Figure S3 demonstrates that the percentage of families that passed the Mann-Kendall test at 95% confidence is high enough to be considered statistically significant at 95% confidence (based on the binomial distribution). The same is true for separate groups of sequences in the north and south.

9. Figure S4 shows that the coefficient of variation (COV) in recurrence interval of the repeating-earthquake sequences is on average 0.4, with only 4 sequences having $COV < 0.1$; i.e., exhibiting near-regular recurrence.

10. Figure S5 shows that the pattern of accelerating recurrence in the south and decelerating recurrence in the north inferred from the Mann-Kendall (MK) test at 95% confidence is consistent with the result of the MK test at 90% confidence (panel a) as well as the Spearman's rank correlation coefficient between recurrence interval and time (panel b).

11. Figure S6 compares the fits of three different models of repeating-earthquake recurrence to the observed variation between recurrence interval and seismic moment, and shows that the Beeler model captures the weak variation for small moments better than the other two models.

12. Figure S7 shows the predicted cumulative slip histories in the repeating-earthquake sequences that passed the Mann-Kendall test and demonstrates that for most sequences modeled afterslip is negligible compared to the total slip.

13. Figure S8 shows a map of cumulative modeled afterslip, after *Johnson et al.* [2013].

14. Figure S9 shows probability density functions of slip accelerations from the repeating-earthquake sequences that passed the Mann-Kendall test (as in Figure 4a, but with each distribution shown in a separate panel).

15. Figure S10 shows the estimated slip acceleration, corrected for afterslip, at the locations of all repeating-earthquake sequences, including those that failed the Mann-Kendall test and demonstrates that we still observe a pattern of mostly negative slip accelerations in the north and positive in the south, albeit with more variability.

16. Figure S11 compares the distributions of slip acceleration on the plate interface inferred from three different regularization schemes in the joint GPS/repeating-earthquake inversion and demonstrates that the minimum-norm and second-order Tikhonov regularization schemes result in artifacts due to inclusion of point constraints from the repeating earthquakes, whereas the local Laplacian regularization yields a more physical distribution.

17. Figure S12 demonstrates the effect of changing the radius involved in the local Laplacian smoothing in the joint GPS/repeating-earthquake inversion.

Text S1.

The original catalog of repeating earthquakes from *Uchida and Matsuzawa* [2013] contains 1515 sequences (Figure S1). We select sequences that satisfy the following criteria:

1. Sequences with at least 4 events in the time period 1996/03/21 to 2011/02/06; i.e., the minimum number required to observe a monotonic change in recurrence interval.

2. Sequences whose events have average magnitude of $M \geq 3$ or larger. If a sequence missed an event smaller than the detection threshold, the sequence would be corrupted. While the completeness threshold in the catalog is $M \geq 2.5$, we are conservative and choose a minimum of $M \geq 3$.

3. Sequences whose events have low variation in magnitude; we use a threshold in the standard deviation of the magnitudes of 0.3 units. If a sequence truly reflects repeating rupture of the same source area, then the magnitudes within the sequences should not vary significantly.

4. Sequences that span a relatively long time within the 15-year period of interest (i.e., “persistent” sequences, as in *Satriano et al.* [2014]). This avoids clusters of repeating events that are short-lived and thus likely to represent rapid slip transients. Specifically, our criterion is that each sequence must satisfy the condition $10 \leq N\bar{T} \leq 30$ yr, where N is the number of events in the sequence during the period of interest and \bar{T} is the average recurrence interval in the sequence (Figure S2).

Text S2.

There are at least two non-parametric statistical tests for detecting monotonic trends in noisy time series data: the Mann-Kendall (MK) test [Mann, 1945; Kendall, 1948] and the Spearman's rho test [Lehmann and D'Abbrera, 2006]. The MK test has been commonly used in detecting trends in hydro-meteorological time series [e.g., Yue *et al.*, 2002]. Simulations demonstrate that the two tests have similar power in detecting a trend, to the point of being indistinguishable in practice [Yue *et al.*, 2002]. In general, passing the MK test (at a predefined confidence level) is a function of three factors: the number of samples, the scatter in the data, and the magnitude of the trend.

The MK test is based on the test statistic S defined as

$$S = \sum_{i=1}^{n-1} \sum_{j=i+1}^n \text{sgn}(x_j - x_i) \quad (\text{S1})$$

where the x_j are the sequential data values in a time series, n is the number of samples, and sgn is the signum function. In our case, x_j are the recurrence intervals in a given sequence of repeating earthquakes in the time period 1996/03/21 to 2011/02/06. The statistic S is approximately normally distributed with mean and variance given by $E[S] = 0$ and

$$\text{Var}[S] = \frac{n(n-1)(2n+5)}{18}, \quad (\text{S2})$$

respectively [Mann, 1945; Kendall, 1948]. In the case of ties ($x_i = x_j$), a correction to the variance is needed; however, no ties exist in sequences of repeating earthquakes. The standardized test statistic Z is given by

$$Z = \begin{cases} \frac{S-1}{\sqrt{\text{Var}[S]}} & \text{if } S > 0 \\ 0 & \text{if } S = 0 \\ \frac{S+1}{\sqrt{\text{Var}[S]}} & \text{if } S < 0 \end{cases} \quad (\text{S3})$$

and follows the standard normal distribution, $Z \sim \mathcal{N}(0, 1)$. The P -value of the MK statistic can be estimated by

$$p = 1 - \Phi(|Z|), \quad (\text{S4})$$

where $\Phi(|Z|)$ is the normal cumulative distribution function of $|Z|$. If the P -value is small enough, the trend is unlikely to be caused by chance. A robust estimate of the (signed) magnitude of the monotonic trend is given by *Sen* [1968] as

$$\beta = \text{Median} \left(\frac{x_j - x_l}{j - l} \right) \quad \forall l < j. \quad (\text{S5})$$

Table S1 lists the sequences of repeating earthquakes that pass the MK test for significant trend in recurrence interval at 95% confidence. 4 sequences have $\beta > 0$ (upward trend in recurrence interval) and 12 sequences have $\beta < 0$ (downward trend in recurrence interval). Note that the 9 sequences with only 4 events that pass the test have a relatively strong trend, while the sequences with more than 4 events have generally weaker (but still significant) trends. Specifically, the average trend magnitude is $\langle |\beta| \rangle = 1.7$ for sequences with 4 events, whereas $\langle |\beta| \rangle = 0.3$ for sequences with more than 4 events.

Text S3.**Standard model**

The first model we consider represents each repeating earthquake as rupture on a circular crack of fixed radius r that undergoes uniform stress drop $\Delta\tau$ in an elastic full-space. The model assumes that all slip at the location of the repeating earthquake is accumulated seismically. Using the definition of seismic moment, $M_0 = \pi\mu sr^2$, where s is the average (seismic) slip and μ is the shear modulus, one can derive the following relationship between recurrence interval, T , and seismic moment:

$$T = \frac{\Delta\tau^{2/3} M_0^{1/3}}{1.81\mu V_L}, \quad (\text{S6})$$

[*Nadeau and Johnson, 1998; Beeler et al., 2001*]. However, the $T \propto M_0^{1/3}$ scaling predicted from this model is inconsistent with observations from northeastern Japan [*Chen et al., 2007*] as well as the San Andreas Fault, California [*Nadeau and Johnson, 1998; Beeler et al., 2001; Chen and Lapusta, 2009*].

Nadeau-Johnson model

The second model we consider is based on the empirical scaling relationship of *Nadeau and Johnson* [1998], who found that $T \propto M_0^{0.17}$ from repeating earthquakes on the Parkfield segment of the San Andreas Fault. The scaling relationship can be written as

$$\log T = \alpha \log M_0 + \beta \quad (\text{S7})$$

where α and β are empirically derived constants, with $\alpha = 0.17$. While this relationship has been applied to repeating earthquakes outside of Parkfield, *Chen et al.* [2007] showed that only after accounting for the differences in regional loading rates did the scaling become consistent with data from Taiwan and NE Japan. Here we follow *Chen et al.* [2007] and adjust the Nadeau-

Johnson scaling to make it applicable for NE Japan by normalizing the Parkfield recurrence interval by the ratio of the Parkfield loading rate, $V_{\text{Parkfield}} = 2.3 \text{ cm/yr}$ [Nadeau and Johnson, 1998], to the NE Japan loading rate, V_L , as follows:

$$T_{\text{Parkfield}}^{\text{norm}} = \frac{V_L}{V_{\text{Parkfield}}} T_{\text{Parkfield}}. \quad (\text{S8})$$

Therefore, the adjusted Nadeau-Johnson scaling that can be used for NE Japan data is

$$\log T = \alpha \log M_0 + \left(\log \frac{V_{\text{Parkfield}}}{V_L} + \beta \right). \quad (\text{S9})$$

However, assuming no aseismic slip, the Nadeau-Johnson predicts extremely high stress drops ($\sim 2500 \text{ MPa}$) for the smallest repeating earthquakes in order to fit the observed recurrence intervals [Nadeau and Johnson, 1998], contrary to subsequent estimates of stress drops of small repeating earthquakes which lie within the typical range of 1 to 10 MPa [Imanishi *et al.*, 2004; Allmann and Shearer, 2007].

Beeler model

Beeler *et al.* [2001] developed an alternative model that allows for aseismic slip as part of the cumulative slip that is accommodated at the source location of a repeating earthquake. The model is based on a spring slider governed by a strain-hardening constitutive law. Because of the strain-hardening property, part of the accumulated slip during each cycle is aseismic, and the ratio of aseismic to total slip is larger for smaller events. The resulting scaling of recurrence time with seismic moment has a trend that is consistent with observations both from the San Andreas Fault [Beeler *et al.*, 2001] and NE Japan [Igarashi *et al.*, 2003]. In addition, the high proportion of aseismic slip in the smaller events results in much more reasonable stress drops compared to the Nadeau-Johnson model [Beeler *et al.*, 2001]. The effect of higher proportion of aseismic slip in smaller events was later supported by numerical simulations using rate-and-

state friction [*Chen and Lapusta, 2009*]. In the Beeler model, which is the third and final model that we consider, recurrence interval is related to seismic moment by

$$T = \frac{\Delta\tau}{V_L} \left[\frac{1}{1.81\mu} \left(\frac{M_0}{\Delta\tau} \right)^{1/3} + \frac{1}{C} \right], \quad (\text{S10})$$

where $\Delta\tau$ is the stress drop and C is the strain-hardening coefficient, which controls the ratio of aseismic to total slip [*Beeler et al., 2001*].

Model selection

We fit each of the three models (equations (S6), (S9), and (S10), respectively) to all 76 individual observations of $\bar{T}(\bar{M}_0)$ (one for each sequence of repeating earthquakes) using a Markov-chain Monte Carlo (MCMC) method. We assume a value for the shear modulus equal to $\mu = 3 \times 10^{10}$ Pa. The standard model (equation (S6)) has two unknown parameters: loading velocity, V_L , and stress drop, $\Delta\tau$. The Nadeau-Johnson model (equation (S9)) has three unknowns, V_L , α , and β , the latter two being the slope and intercept in the original Nadeau-Johnson model, respectively. Finally, the Beeler model (equation (S10)) has three unknown parameters, V_L , $\Delta\tau$, and C , the strain-hardening coefficient. We use uniform priors for all unknown parameters, except for the Nadeau-Johnson constants, for which we use Gaussian priors with means and standard errors taken from the values given in *Nadeau and Johnson [1998]*. Additionally, we bound V_L between 0 and 8.3 cm/yr, the long-term plate convergence rate in NE Japan [*DeMets et al., 2010*].

Figure S6 shows the results of fitting the three models to the observations of $\bar{T}(\bar{M}_0)$. The standard model, having a slope of $\frac{1}{3}$ in logarithmic space, is inconsistent with the observed weak variation between \bar{T} and \bar{M}_0 , as pointed out by other studies [*Beeler et al., 2001; Chen and Lapusta, 2009*]. In contrast, both the Nadeau-Johnson and Beeler models fit the observa-

tions considerably better. We compute Akaike information criterion (AIC) [*Akaike*, 1974] and Bayesian information criterion (BIC) [*Schwarz*, 1978] statistics for each model and find the following: The AIC statistics are 23.1 for the standard model, 19.6 for the Nadeau-Johnson model, and 18.5 for the Beeler model. The BIC statistics are 18.4 for the standard model, 12.6 for the Nadeau-Johnson model, and 11.5 for the Beeler model. Therefore, the Nadeau-Johnson and Beeler models give a significantly better fit to the data compared to the standard model, with the Beeler model having the lowest values of both BIC and AIC, although not very different from the Nadeau-Johnson model. We therefore adopt the Beeler model for calculating slip as a function of moment.

Text S4.

Inversion setup

We use the same plate interface model as in *Mavrommatis et al.* [2014] and relate the accelerations in GPS time series to slip acceleration on the plate interface as

$$\mathbf{d} = \mathbf{G}\mathbf{m} + \boldsymbol{\varepsilon} \quad (\text{S11})$$

where \mathbf{d} is a vector of observed GPS station accelerations, \mathbf{m} is the $(M \times 1)$ vector of unknown slip acceleration values on M fault patches, \mathbf{G} is a matrix of Green's functions mapping slip on triangular patches to surface displacements [Meade, 2007], and $\boldsymbol{\varepsilon} \sim \mathcal{N}(\mathbf{0}, \boldsymbol{\Sigma})$ is a random error vector that follows a normal distribution with zero mean and covariance matrix $\boldsymbol{\Sigma}$. A discussion of how $\boldsymbol{\Sigma}$ is estimated is provided the subsection "Estimating correlations in GPS station accelerations".

We use the GPS station accelerations and the estimates of slip acceleration at the locations of the repeating earthquakes jointly to estimate the distribution of slip acceleration everywhere on the megathrust by solving the minimization problem

$$\min_{\mathbf{m}} \left[\|\boldsymbol{\Sigma}^{-1/2}(\mathbf{d} - \mathbf{G}\mathbf{m})\|_2^2 + \|\mathbf{C}^{-1/2}(\mathbf{H}\mathbf{m} - \mathbf{m}^*)\|_2^2 + \alpha^2 \|\mathbf{D}\mathbf{m}\|_2^2 \right]. \quad (\text{S12})$$

The first term penalizes misfit to the observed GPS station accelerations. The second term penalizes misfit to the estimates of slip acceleration at the locations of the repeating earthquake sequences: \mathbf{m}^* is an $(N_c \times 1)$ vector of the modes of the slip acceleration PDFs corresponding to the $N_c = 16$ patches whose centroids are closest to the locations of the repeating earthquakes that passed the MK test, \mathbf{H} is an $(N_c \times M)$ index matrix such that its j th column is \mathbf{e}_k , $k = 1, \dots, N_c$ if $j = k$ and $\mathbf{0}$ otherwise, where \mathbf{e}_k is the k th column of the $(N_c \times N_c)$ identity matrix, and \mathbf{C} is an $(N_c \times N_c)$ diagonal covariance matrix containing the sample variances of

the PDFs of slip accelerations inferred from the repeating earthquakes. Finally, the last term is a regularization term that minimizes the variance of \mathbf{m} given some operator \mathbf{D} (e.g., for minimum norm, $\mathbf{D} = \mathbf{I}$ and for second-order Tikhonov regularization, $\mathbf{D} = \mathbf{L}$, the finite-difference approximation of the Laplacian operator). A discussion of how \mathbf{D} is chosen is provided in the subsection “Model regularization”. The scalar α^2 places a relative weight between fitting the data (both GPS and repeating earthquakes) versus regularizing the model estimate. The value of α^2 is chosen empirically using a tradeoff curve between the data misfit (first two terms in equation (S12)), and the model roughness, $\|\mathbf{D}\mathbf{m}\|_2^2$.

Estimating correlations in GPS station accelerations

Geodetic data are known to be spatially correlated [Lohman and Simons, 2005]. To estimate the covariance matrix of the GPS station accelerations, Σ , we compute the spatial autocorrelation function of the residual GPS accelerations, $\mathbf{r} = \mathbf{d} - \mathbf{G}\hat{\mathbf{m}}$, given a model estimate $\hat{\mathbf{m}}$. We define the spatial autocorrelation function as the covariance of the residual GPS acceleration between each station and all stations that are located at some distance away. Assuming the mean of the residuals is spatially uniform, the autocorrelation as a function of lag distance h_k is given by

$$C(h_k) = \frac{1}{N_k} \sum_{i=1}^{N_s} \sum_{j \in \mathcal{J}_k^{(i)}} (r_i - \bar{r})(r_j - \bar{r}) \quad (\text{S13})$$

where \bar{r} is the sample mean of the residuals, i indexes over all N_s stations, and j indexes the stations in the set $\mathcal{J}_k^{(i)}$ defined as the set of stations whose distance from station i is in the range set by the k th lag bin; i.e.,

$$\frac{1}{2}(h_{k-1} + h_k) \leq d_j^{(i)} < \frac{1}{2}(h_k + h_{k+1}) \quad (\text{S14})$$

where $d_j^{(i)}$ is the distance from station i to station j . Finally, N_k is the total number of stations for the k th lag bin; i.e.,

$$N_k = \sum_{i=1}^{N_s} N_k^{(i)} \quad (\text{S15})$$

where $N_k^{(i)}$ is the number of elements in $\mathcal{J}_k^{(i)}$. Assuming spatially uniform variance, we normalize the autocorrelation by the sample variance of the residuals:

$$\hat{C}(h_k) = \frac{C(h_k)}{\text{Var}(r)}. \quad (\text{S16})$$

We model the normalized spatial autocorrelation, $\hat{C}(h_k)$, as an exponentially decaying function with a characteristic decay distance h_c and unit amplitude (since by definition $\hat{C}(0) = 1$):

$$\hat{C}(h) = \exp(-h/h_c). \quad (\text{S17})$$

We then populate the estimated covariance matrix $\hat{\Sigma}$ as

$$\hat{\Sigma}_{ij} = \text{Var}(r) \exp(-d_j^{(i)}/h_c) \quad (\text{S18})$$

This definition produces a symmetric positive definite matrix with constant diagonal.

We employ an iterative procedure, starting with an initial guess of $\hat{\Sigma}_0 = \text{diag}(\sigma^2)$, where σ^2 is the vector of formal variances of the GPS station accelerations, derived from the time-series analysis [Mavrommatis et al., 2014]. After performing the inversion once, we obtain the data residuals r_0 , which are then used to obtain a new estimate of the covariance matrix, $\hat{\Sigma}_1$, according to the method described above. We iterate this procedure until convergence. Using the local Laplacian regularization (see discussion below), we find characteristic correlation distances of $h_c = 24$ km for the east component and $h_c = 43$ km for the north component.

Model regularization

Using either minimum-norm or second-order Tikhonov regularization everywhere on the fault produces solutions that contain artifacts due to the inclusion of the point constraints from the repeating earthquakes (Figure S11). Instead, we perform a mixed minimum-norm/Tikhonov regularization, which we refer to as “local Laplacian regularization”, by imposing second-order Tikhonov regularization on patches that are located within some radius r from each repeating earthquake and minimum-norm regularization everywhere else. The rationale here is that repeating earthquakes reflect slip locally on the fault, which should be spatially smooth, but we conservatively minimize slip acceleration outside these areas to the lowest amplitude required to fit the GPS data. This results in a slip distribution that is locally smooth around the repeating earthquakes (Figure S11c).

Increasing the radius r of the area around each repeating earthquake location for which Laplacian smoothing is imposed results in overall smoother slip-acceleration distributions (Figure S12). One can place an upper bound on r based on the area of the fault that consists of locked asperities. Using the asperity model of *Johnson et al.* [2013], we assume the total area covered by asperities, A_{lock} , remains locked throughout the entire 15-year observation period, hence the area allowed to creep is $A_{\text{creep}} = A_{\text{tot}} - A_{\text{asp}}$, where A_{tot} is the total fault area. We estimate a conservative upper bound on r by assuming A_{creep} is distributed over N disjoint circles, where $N = 16$ is the number of repeating earthquake sequences that passed the MK test; i.e., $r_{\text{max}} = \sqrt{A_{\text{creep}}/(N\pi)}$. Using this approximation, we find $r_{\text{max}} = 49$ km. On the other hand, a lower bound on r can be placed by assuming the average slip rate never exceeds the plate rate of 8.3 cm/yr [*DeMets et al.*, 2010] in the 15-year observation period

(since decreasing r results in higher amplitude of slip acceleration). For example, assuming the plate interface was fully locked at the beginning of the observation period, the average acceleration so that the plate rate is not exceeded at the end of the observation period (14.6 years) is $a_{\max} = (8.3 \text{ cm/yr})/(14.6 \text{ yr}) = 5.7 \text{ mm/yr}^2$; we find that this bound is satisfied for all $r > 30 \text{ km}$, but using this value as a bound on the maximum, instead of average, acceleration, places a lower bound on r of 52 km (Figure S12). We therefore choose $r = 50 \text{ km}$ as a reasonable scenario.

References

- Akaike, H. (1974), A new look at the statistical model identification, *Automatic Control, IEEE Transactions on*, 19(6), 716–723, doi:10.1109/TAC.1974.1100705.
- Allmann, B. P., and P. M. Shearer (2007), Spatial and temporal stress drop variations in small earthquakes near Parkfield, California, *Journal of Geophysical Research: Solid Earth*, 112(B4), doi:10.1029/2006JB004395.
- Beeler, N., D. Lockner, and S. Hickman (2001), A simple stick-slip and creep-slip model for repeating earthquakes and its implication for microearthquakes at Parkfield, *Bulletin of the Seismological Society of America*, 91(6), 1797–1804, doi:10.1785/0120000096.
- Chen, K. H., R. M. Nadeau, and R.-J. Rau (2007), Towards a universal rule on the recurrence interval scaling of repeating earthquakes?, *Geophysical Research Letters*, 34(16), doi:10.1029/2007GL030554.
- Chen, T., and N. Lapusta (2009), Scaling of small repeating earthquakes explained by interaction of seismic and aseismic slip in a rate and state fault model, *Journal of Geophysical Research: Solid Earth*, 114(B1), doi:10.1029/2008JB005749.

- DeMets, C., R. G. Gordon, and D. F. Argus (2010), Geologically current plate motions, *Geophysical Journal International*, 181(1), 1–80, doi:/10.1111/j.1365-246x.2009.04491.x.
- Igarashi, T., T. Matsuzawa, and A. Hasegawa (2003), Repeating earthquakes and interplate aseismic slip in the northeastern Japan subduction zone, *Journal of Geophysical Research: Solid Earth*, 108(B5), doi:10.1029/2002JB001920.
- Imanishi, K., W. L. Ellsworth, and S. G. Prejean (2004), Earthquake source parameters determined by the SAFOD Pilot Hole seismic array, *Geophysical Research Letters*, 31(12), doi:10.1029/2004GL019420.
- Johnson, K. M., A. P. Mavrommatis, and P. Segall (2013), Overlapping afterslip and coseismic slip on the Northern Japan subduction interface inferred from physical models of slip and GPS time series from 2003-2011, Abstract G31C-06 presented at 2013 Fall Meeting, AGU, San Francisco, CA, 9-13 December.
- Kendall, M. G. (1948), *Rank correlation methods*, Griffin, Oxford, England, doi:10.2307/2333282.
- Lehmann, E. L., and H. J. D’Abrera (2006), *Nonparametrics: statistical methods based on ranks*, Springer New York.
- Lohman, R. B., and M. Simons (2005), Some thoughts on the use of InSAR data to constrain models of surface deformation: Noise structure and data downsampling, *Geochemistry, Geophysics, Geosystems*, 6(1), doi:10.1029/2004gc000841.
- Mann, H. B. (1945), Nonparametric tests against trend, *Econometrica: Journal of the Econometric Society*, pp. 245–259, doi:10.2307/1907187.

- Mavrommatis, A. P., P. Segall, and K. M. Johnson (2014), A decadal-scale deformation transient prior to the 2011 Mw 9.0 Tohoku-oki earthquake, *Geophysical Research Letters*, *41*(13), 4486–4494, doi:10.1002/2014gl060139.
- Meade, B. J. (2007), Algorithms for the calculation of exact displacements, strains, and stresses for triangular dislocation elements in a uniform elastic half space, *Computers & geosciences*, *33*(8), 1064–1075, doi:10.1016/j.cageo.2006.12.003.
- Nadeau, R. M., and L. R. Johnson (1998), Seismological studies at Parkfield VI: Moment release rates and estimates of source parameters for small repeating earthquakes, *Bulletin of the Seismological Society of America*, *88*(3), 790–814.
- Satriano, C., V. Dionicio, H. Miyake, N. Uchida, J.-P. Vilotte, and P. Bernard (2014), Structural and thermal control of seismic activity and megathrust rupture dynamics in subduction zones: Lessons from the Mw 9.0, 2011 Tohoku earthquake, *Earth and Planetary Science Letters*, *403*, 287–298, doi:10.1016/j.epsl.2014.06.037.
- Schwarz, G. (1978), Estimating the dimension of a model, *The annals of statistics*, *6*(2), 461–464, doi:10.1214/aos/1176344136.
- Sen, P. K. (1968), Estimates of the regression coefficient based on Kendall's tau, *Journal of the American Statistical Association*, *63*(324), 1379–1389, doi:10.2307/2285891.
- Uchida, N., and T. Matsuzawa (2013), Pre-and postseismic slow slip surrounding the 2011 Tohoku-oki earthquake rupture, *Earth and Planetary Science Letters*, *374*, 81–91, doi:10.1016/j.epsl.2013.05.021.
- Yue, S., P. Pilon, and G. Cavadias (2002), Power of the Mann–Kendall and Spearman's rho tests for detecting monotonic trends in hydrological series, *Journal of Hydrology*, *259*(1),

254–271, doi:10.1016/s0022-1694(01)00594-7.

Table S1. Statistics of sequences of repeating earthquakes that pass the Mann-Kendall test for significant trend in recurrence interval at 95% confidence.

Number	ID	N^a	\bar{T}^b	β^c	P -value
1	387	10	1.41	0.08	0.0165
2	432	9	1.63	0.23	0.0354
3	557	7	2.28	0.18	0.0085
4	569	10	1.51	0.06	0.0165
5	805	7	2.03	-0.36	0.0026
6	890	5	3.04	-1.09	0.0174
7	931	4	3.26	-1.22	0.0367
8	987	9	1.80	-0.12	0.0044
9	992	4	3.85	-1.95	0.0367
10	1042	4	3.60	-0.32	0.0367
11	1099	4	2.99	-0.88	0.0367
12	1165	4	3.07	-1.33	0.0367
13	1227	4	3.28	-1.89	0.0367
14	1409	4	3.96	-2.14	0.0367
15	1411	4	3.81	-3.02	0.0367
16	1475	4	4.32	-2.57	0.0367

^a Number of events in sequence

^b Average recurrence interval in years

^c Magnitude of the trend, given by equation (S5) (dimensionless)

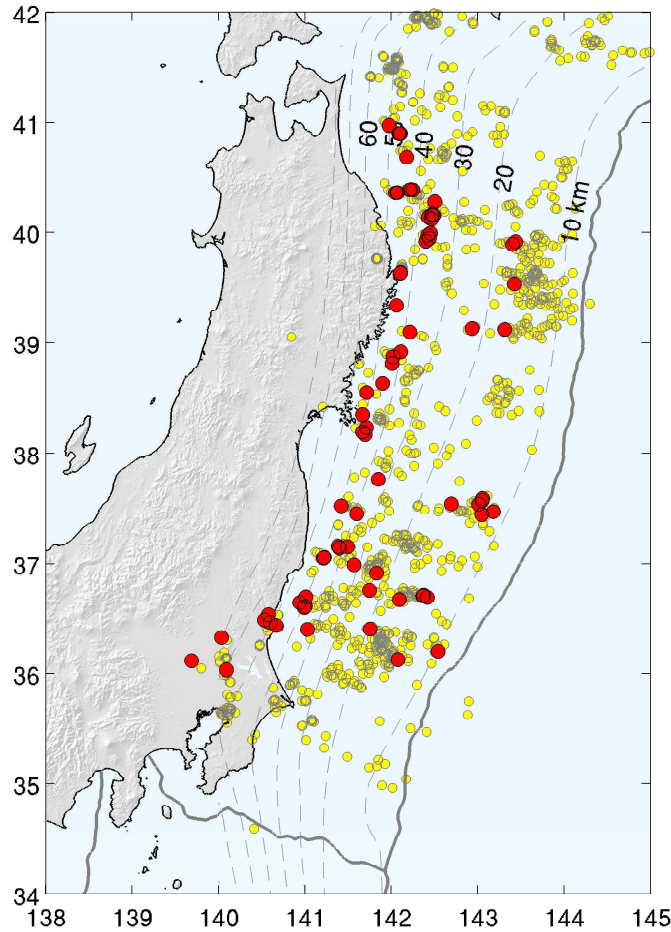


Figure S1. Epicentral distribution of families of repeating earthquakes. Yellow circles are the epicentral locations of families from the catalog of *Uchida and Matsuzawa* [2013] (each family location is taken as the average location of the earthquakes within that family). Red circles show the selected families used in this study (see Text S1 for details on selection criteria).

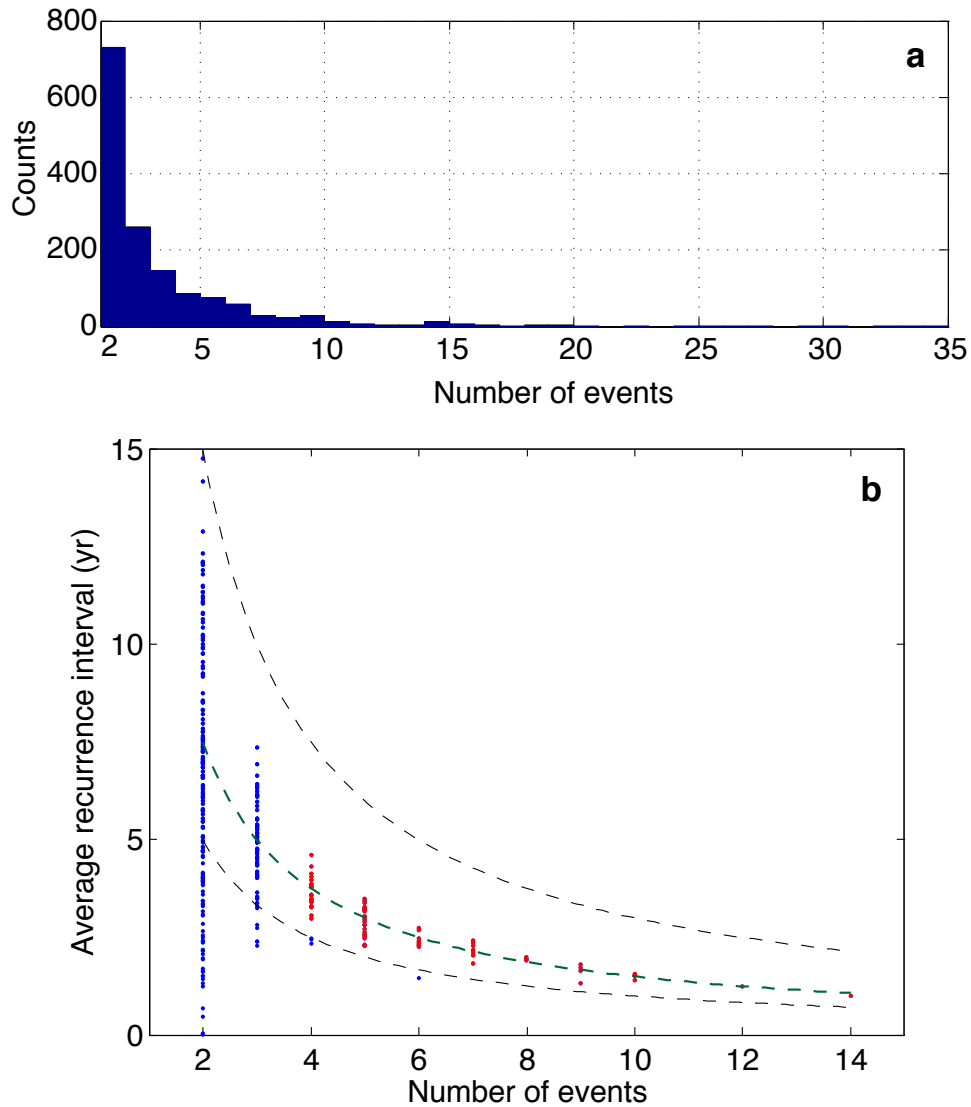


Figure S2. (a) Distribution of number of events per sequence in the catalog of repeating earthquakes [Uchida and Matsuzawa, 2013]. (b) Selection of “persistence” thresholds for repeating earthquake sequences based on each sequence’s number of events, N , and average recurrence interval, \bar{T} [as in Satriano et al., 2014]. Green dashed line satisfies $N\bar{T} = 15$ yr; dashed black curves are upper and lower bounds of 30 yr and 10 yr, respectively. Dots correspond to all sequences in the catalog. Only sequences falling in the bounded region and with $N \geq 4$ (red dots) are included in the analysis.

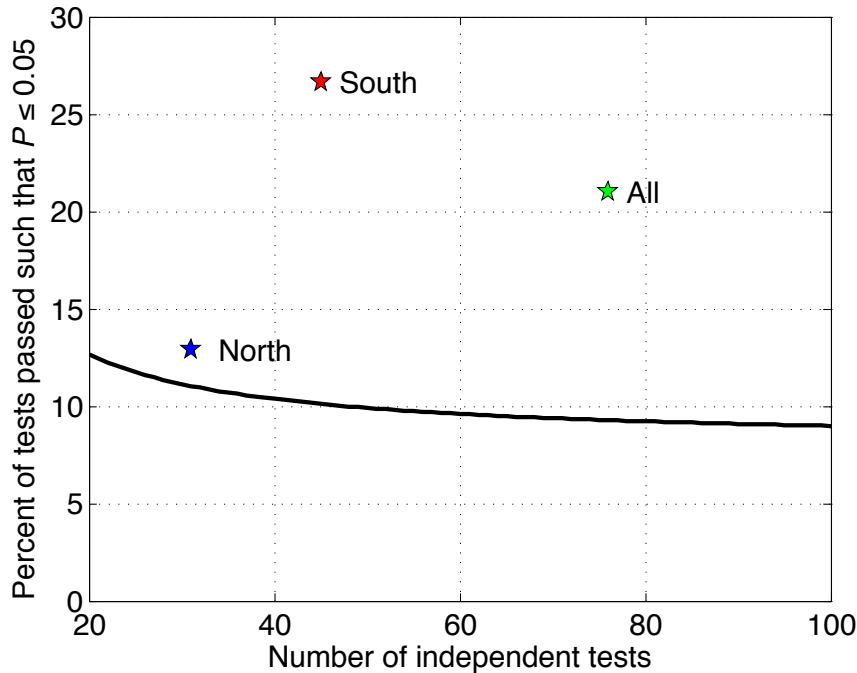


Figure S3. Test for collective significance of trends in recurrence intervals of repeating earthquake sequences. The figure plots the percent of independent 95% significant tests passed that will be equalled or exceeded by random chance 5% of the time versus the number of independent tests (black curve). The curve is derived from the binomial distribution. Points above the curve correspond to significance tests that are also collectively significant; points below the curve correspond to tests that are not collectively significant. The plotted stars correspond to the Mann-Kendall tests for all repeating earthquake sequences (green), sequences in the north (blue), and sequences in the south (red).

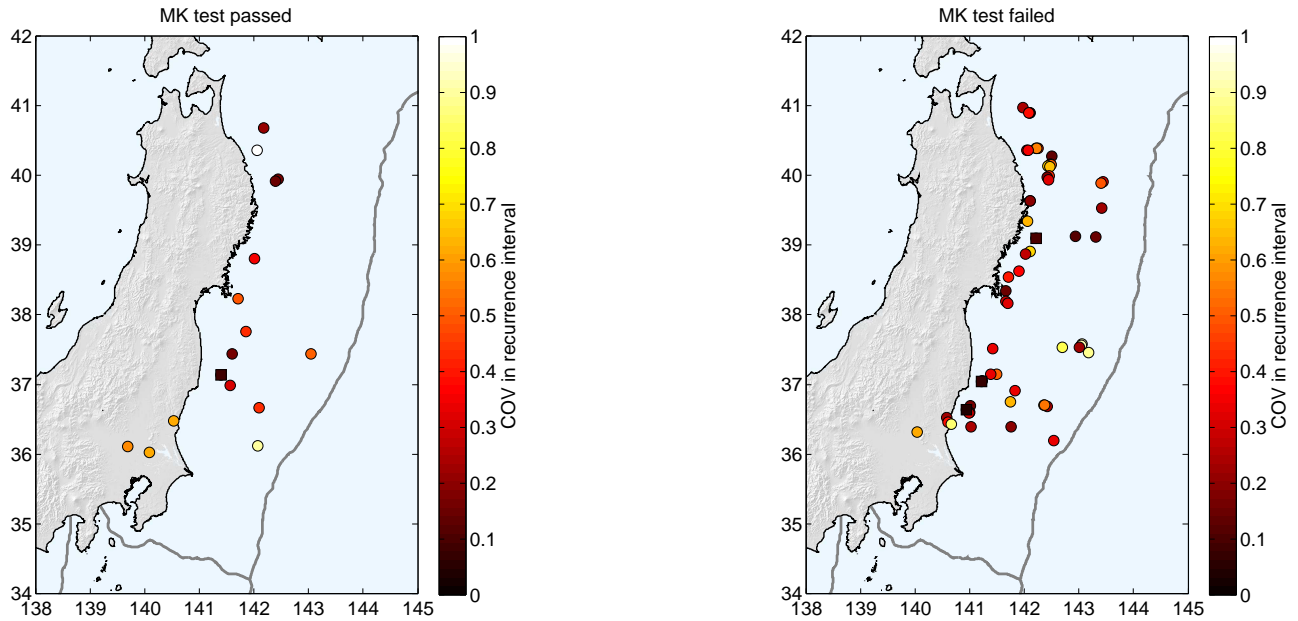


Figure S4. Coefficients of variation (COV) in the recurrence interval of sequences of repeating earthquakes. Panels correspond to sequences that either passed (left) or failed (right) the Mann-Kendall test for significant trends in recurrence interval. Squares correspond to sequences for which $\text{COV} < 0.1$ (near-regular recurrence).

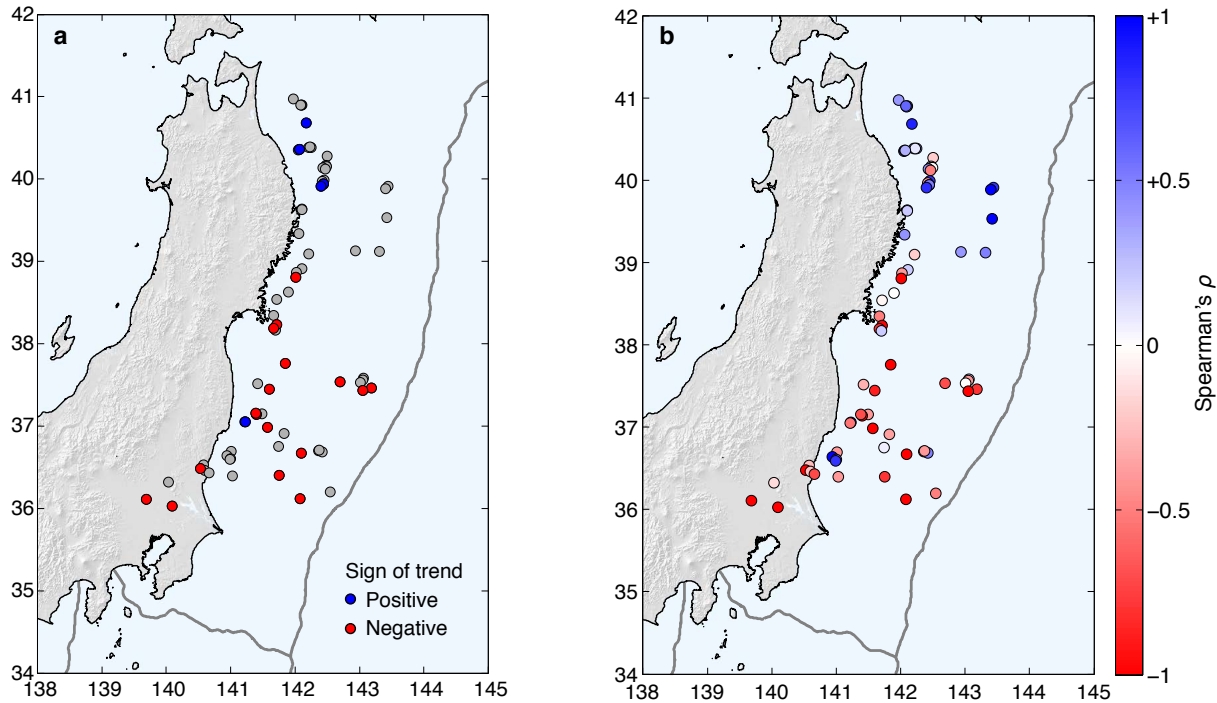


Figure S5. (a) Result of the Mann-Kendall test for significant trends in recurrence interval at 90% confidence. Sequences that pass the test and have positive trends in recurrence interval (decelerating recurrence) are shown in blue; sequences that pass the test and have negative trends (accelerating recurrence) in red. Sequences that fail the test are shown in grey. (b) Spearman's rank correlation coefficient, ρ , between recurrence interval and time for each of the repeating-earthquake sequences. A value of $\rho = 0$ indicates that there is no tendency for the recurrence interval to increase or decrease with time (i.e., no significant trend, implying either regular or Poissonian recurrence). If $\rho > 0$, recurrence interval tends to increase monotonically with time (decelerating recurrence) and if $\rho < 0$, recurrence interval tends to decrease monotonically with time (accelerating recurrence). The cases $\rho = +1$ and $\rho = -1$ indicate perfect positive and negative monotonic trends, respectively.

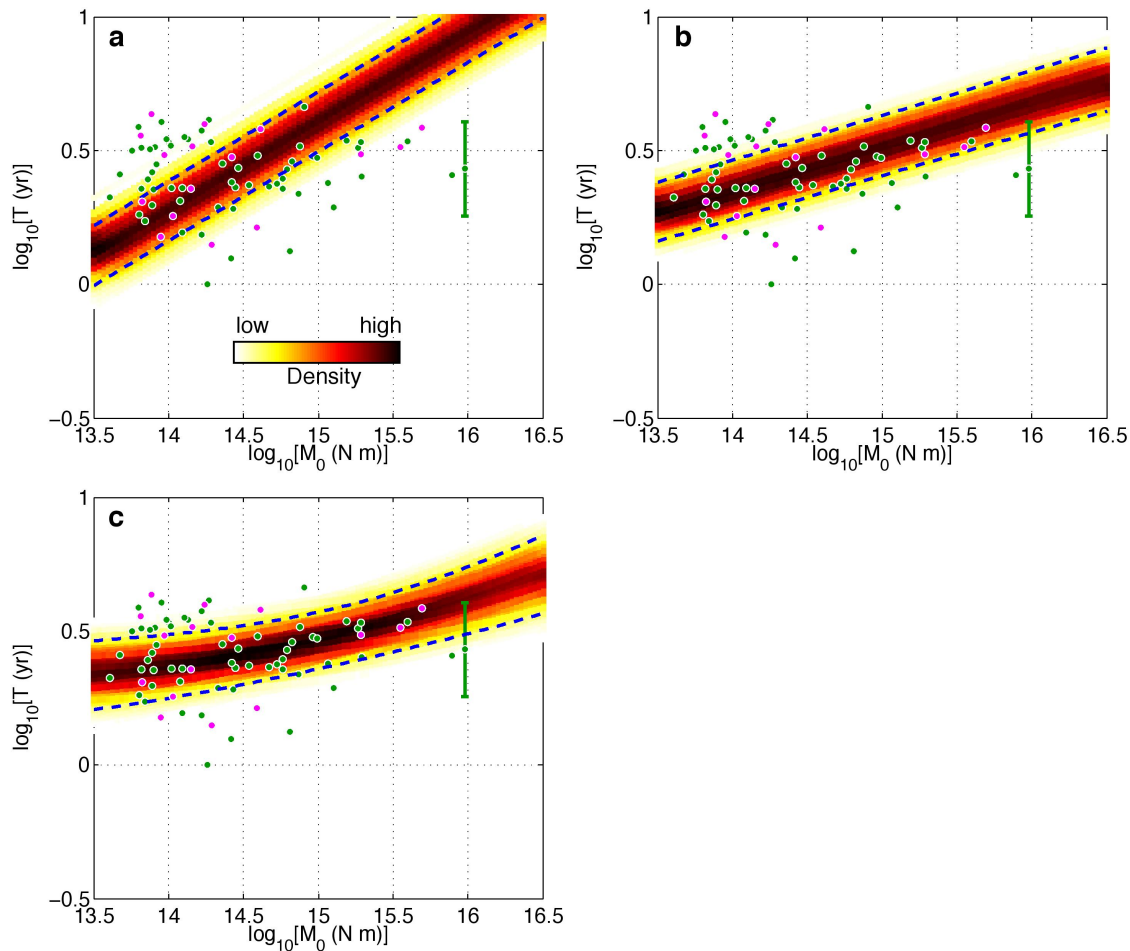


Figure S6. Fits of three different recurrence models to the observed variation between recurrence interval (T) and seismic moment (M_0) of repeating earthquakes: (a) standard model, (b) Nadeau-Johnson model, (c) Beeler model. Dots plot average recurrence intervals and moments of the 76 sequences of repeating earthquakes that passed our selection criteria (sequences that failed the MK test in green, those that passed in magenta). Background color in each panel corresponds to the density of fitted curves from an ensemble produced by MCMC sampling. Blue dashed curves are 95% confidence limits. Error bars indicate average standard deviation in recurrence interval.

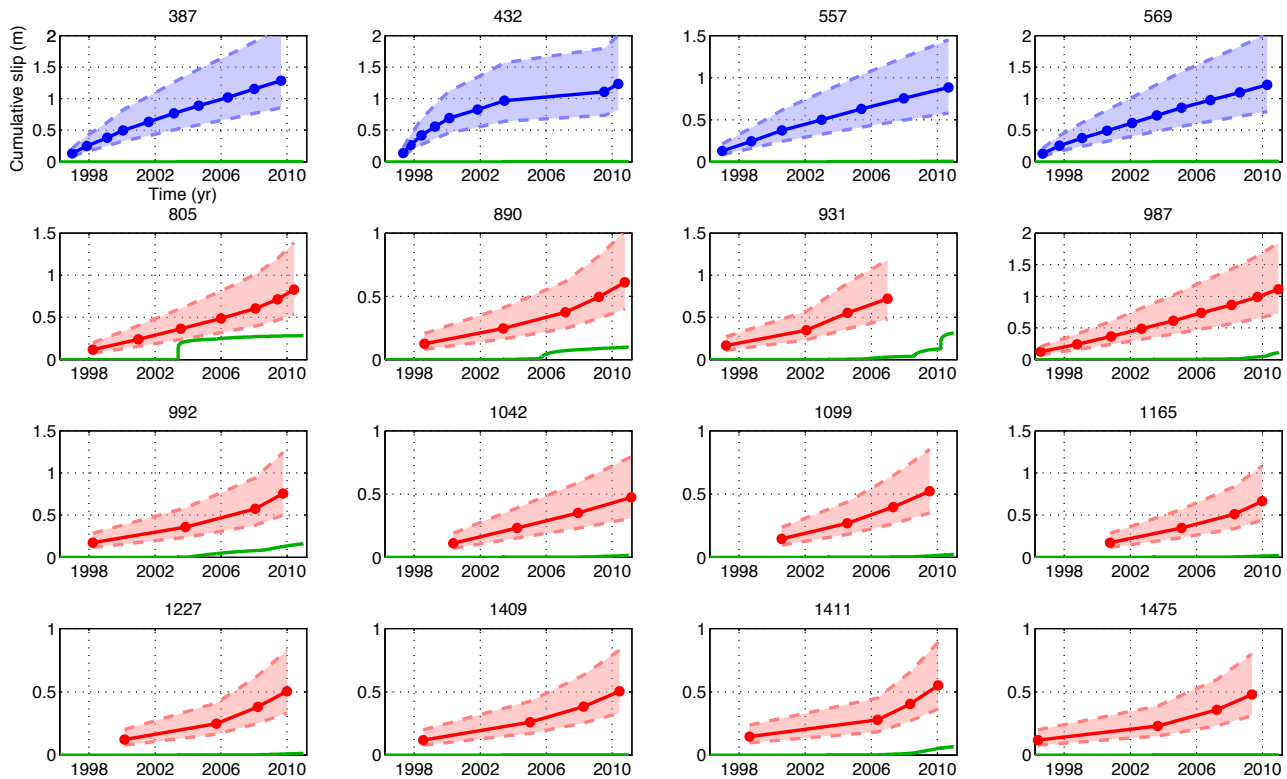


Figure S7. Panels show the ensemble of predicted cumulative slip histories in each sequence that passed the Mann-Kendall test for significant trend in recurrence interval (blue for sequences with positive trends in recurrence interval, red for negative). Solid blue and red curves are the means of all realizations in each ensemble and shaded regions bounded by dashed lines show the region of 95% of all realizations. (Note that this does not imply that any trajectory through the shaded regions is possible, such as a straight line. In fact, the vast majority of realizations in each panel exhibit consistent curvature; i.e., change in slip rate.) Modeled cumulative afterslip at the location of each repeating sequence is shown by the green curves. The locations of the sequences are shown in Figure 1a in the text.

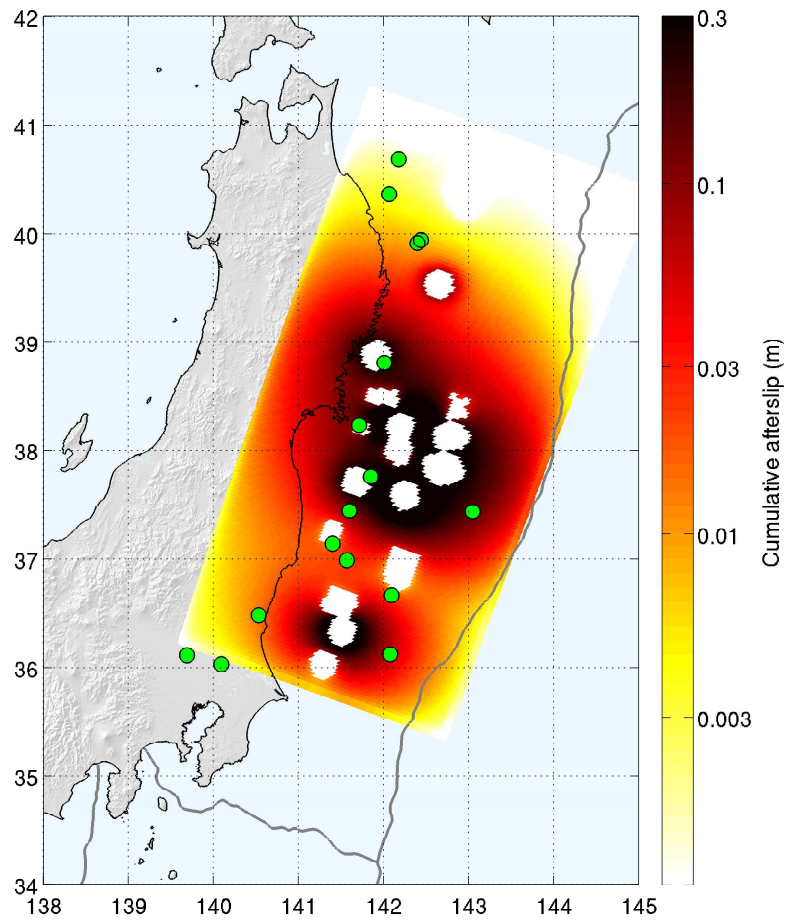


Figure S8. Map of cumulative modeled afterslip for the time interval 1996–2011 (before the Tohoku-oki earthquake) from *Johnson et al.* [2013]. Green circles are locations of the repeating earthquake sequences that passed the MK test.

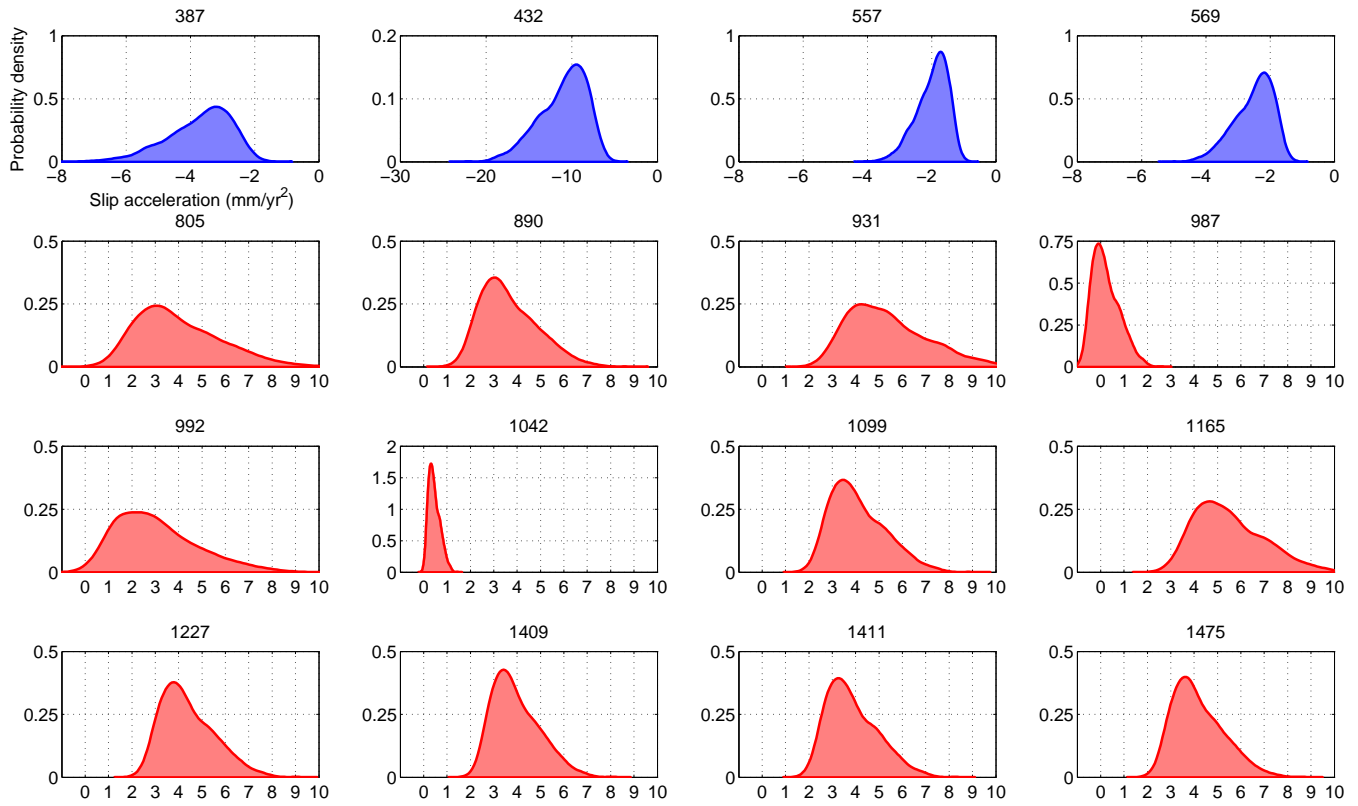


Figure S9. Probability density functions of slip accelerations from the sequences of repeating earthquakes that passed the MK test for significant trends in their recurrence intervals (blue for positive trend, red for negative), corrected for afterslip. The locations of the sequences are shown in Figure 1a in the text.

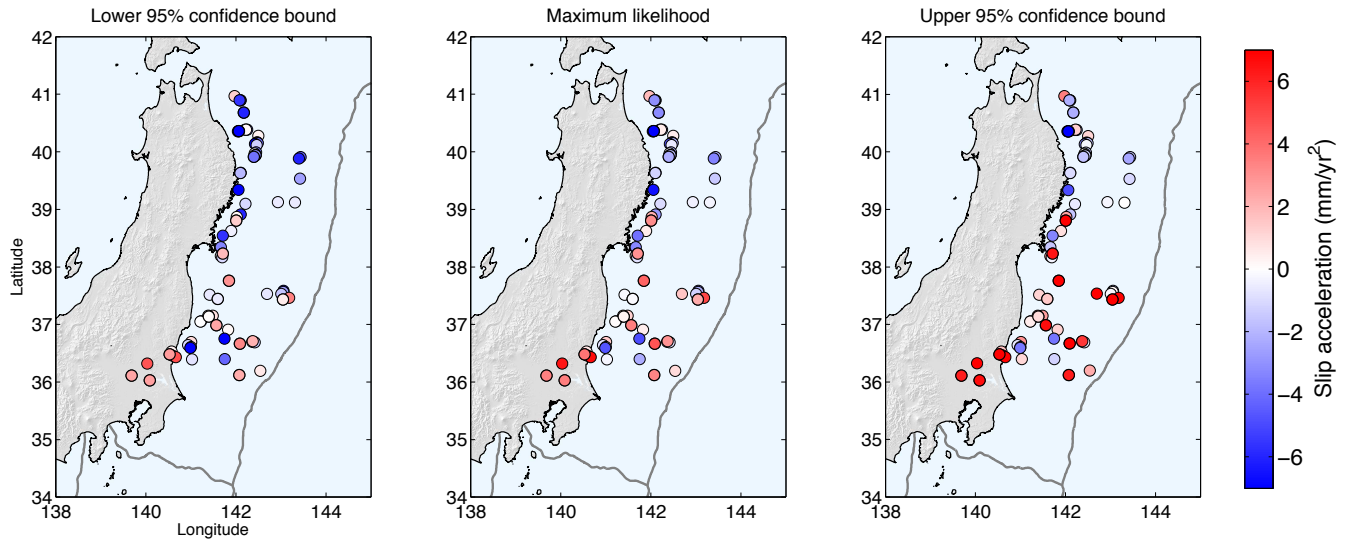


Figure S10. Spatial distribution of estimated slip acceleration on the plate interface, corrected for afterslip, at the locations of all 76 sequences of repeating earthquakes, including those that failed the Mann-Kendall test for significant trends in recurrence interval. Panels correspond to lower 95% confidence bounds (left), maximum-likelihood values (center), and upper 95% confidence bounds (right).

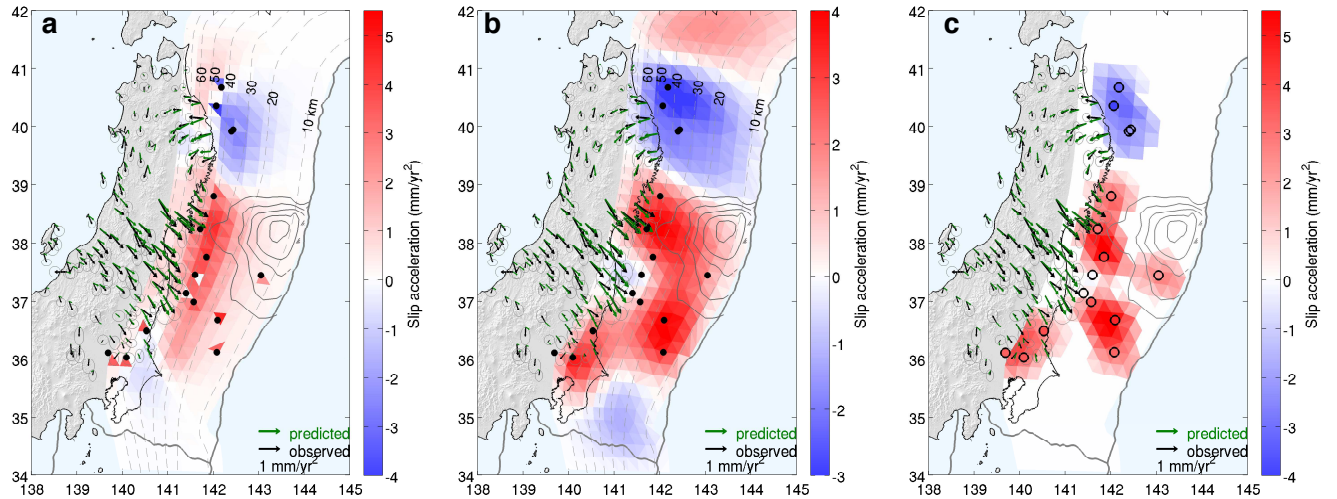


Figure S11. Results of joint GPS/repeating-earthquake inversion using three different regularization schemes: (a) minimum norm, (b) Laplacian smoothing, and (c) local Laplacian smoothing. Black and green arrows are observed and predicted accelerations in GPS time series, respectively. Colors (blue to red) show the magnitude of estimated slip acceleration on the plate interface. Black dots in a and b are the locations of the repeating earthquake sequences that passed the MK test and colored circles in c show the magnitude of slip acceleration estimated at those locations.

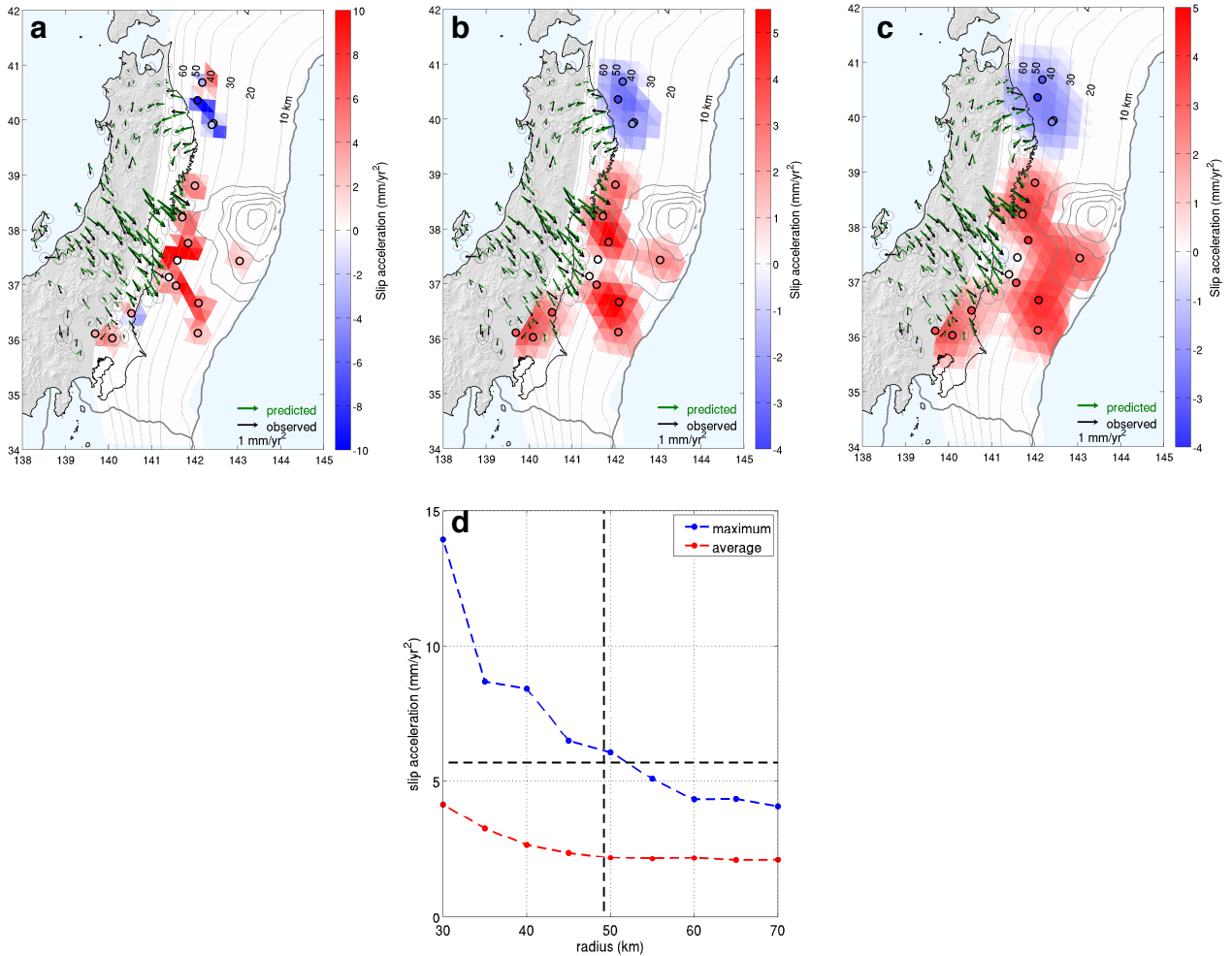


Figure S12. Effect of increasing the radius r of the local Laplacian smoothing in the joint GPS/repeating-earthquake inversion. (a-c) Modeled slip acceleration distributions corresponding to $r = 30$ km (a), $r = 50$ km (b), and $r = 70$ km (c), respectively. Symbols and colors as in Figure S11c. Note differences in color scale. (d) Tradeoff between radius of the local Laplacian smoothing (r) and estimated slip acceleration (maximum in blue, average in red). Vertical dashed line is an approximate upper bound to the radius based on the area of the plate interface that should remain locked at all times; horizontal dashed line is an upper bound on the local slip acceleration based on the constraint that slip rate should never exceed the plate rate.